ELSEVIER

Cement & Concrete Composites 23 (2001) 33–45

Cement & Concrete Composites

www.elsevier.com/locate/cemconcomp

Delamination in composite plates: influence of shear deformability on interfacial debonding

Domenico Bruno *, Fabrizio Greco

Department of Structural Engineering, University of Calabria, 87030 Arcavacata Rende, Cosenza, Italy

Received 7 June 2000; accepted 7 November 2000

Abstract

An elastic interface model is introduced to investigate the effects of in-plane and out-plane shear stresses on interfacial debonding in laminated composite plates by means of the energy release rate concept. This is done by utilising an improved laminated plate model in which the Reissner–Mindlin kinematics type for each layers is coupled with an adhesion mechanism modelled by means of a linear interface model, acting in the opening and sliding failure mode directions. The problem is faced through an analytical solution procedure. Increasing the stiffnesses of the interface leads to restoring displacement continuity at the interface between layers and to recovering energy release rate components through the work performed by the singular stress field at the crack tip. In view of the great importance of shear deformation in laminated composite plates the effect of shear stresses on the mechanism of delamination are investigated pointing out new features which emerge from the interaction of normal and shear stresses acting on the transverse section near the crack tip. Several examples of mixed mode delamination schemes used in experimental applications are examined, showing the influence of transverse shear stresses in coupling with normal stresses on energy release rates determination.

Keywords: Composites; Layered plates; Delamination; Interface model; Coupling effects

1. Introduction

Nowadays the utilisation of composite materials, especially in the form of fiber-reinforced plastics, cement composites and wood composites, is a reality in many kinds of structural applications. As a matter of fact, composite structures exhibit notable mechanical properties, and they have considerable lightness, durability and strength characteristics. However, there are many degradation phenomena which must be accounted for properly in respect of design laminated composite structures. Delamination is one of the main forms of damage in laminated composites and can arise from various causes such as technological imperfections, stress concentration near geometrical/material discontinuity and local or global buckling of plies [1,2]. A common damage phenomenon which occurs in the repair or rehabilitation of existing structures is debonding between fiber-reinforced plastic sheets and the concrete interface [3]. An appropriate study of this phenomenon is thus needed to avoid the efficacy of the reinforcement provided by composite material being compromised.

Delamination analysis can be simplified because it is assumed that an initial interlaminar defect propagates in its own plane. This is commonly satisfied since the toughness of the interface is relatively low in comparison to that of the adjoining material.

Since the crack is assumed to grow along the interface between two elastic layers the criterion for crack advance along the interface can be analysed by means of a model based on the energy release rate concept. The energy release rate for crack advance in the interface can be expressed as $G = G_{\mathrm{I}} + G_{\mathrm{II}}$, where G_{I} and G_{II} energy release rate components can be defined as the work of the normal and shear stresses acting on the interface through their respective crack face displacements as the crack advances.

In many cases Griffith's criterion is inadequate to accurately predict the growth of delamination when mixed mode loading is involved in interlaminar crack advance [4]. For these cases, some fracture criteria have

* Corresponding author. Tel.: +390-984-494027; fax: +390-984-494045.

E-mail address: d.bruno@unical.it (D. Bruno).

0958-9465/01/$ - see front matter
PII: S0958-9465(00)00068-8

been proposed taking into account the experimental evidence of the different amount of energy required for mode I and mode II delamination [5]. Moreover, a great effort has been made to obtain mode partition by using fracture mechanics concepts coupled with the exact numerical solution for particular loading cases [6,7] or by using interface models in conjunction with simplified structural models for the layers [8].

An analysis of the mode partition of the energy release rate has been developed [9] by using only the classical beam theory but, except for very particular cases, generally the procedure utilised leads to imprecise results.

Moreover, for the double cantilever beam scheme, some simplified models based on beam or plate theory were introduced [10,11], where the adhesion between layers was modelled by means of an elastic foundation or where a refined plate theory was used to model the layers. A similar approach was used in [12], where elastic springs were introduced to analyse a two-dimensional mode I delamination problem by also using an FEM procedure.

As far as the classical plate theory is adopted to evaluate the fracture energies of a delaminated plate, the effects of actual deformations and of interlaminar stresses at the crack tip are neglected. In fact, the importance of shear deformations in composite laminates is well-known and analyses such as those contained in [6,7], devoted to the local problem of a small plate element containing the delamination front, cannot easily be extended to include shear effects, being limited to axial and bending loading conditions.

In this work an improvement on the technique of energy release rates evaluation is presented, introducing a simple linear interface model whose constitutive relation connects opening and sliding displacement jumps to normal and shear interlaminar stresses acting on the interface. Utilising a layer-wise kinematics in which shear deformability is accounted for, in conjunction with the above mentioned linear interface model leads to obtaining an accurate evaluation of interlaminar fracture energies. Interface stiffnesses are treated as penalty parameters to impose displacement continuity at the interface between the layers: this allows us to investigate the singular behaviour of interlaminar stresses in proximity of the delamination tip. The above modelling is able to capture the effects of shear stresses and their interaction with the normal ones.

An analytical solution procedure of the relevant governing equations, coupled with a limit process is employed to obtain the fracture energy aliquots of mode I and mode II, essentials for predicting delamination growth behaviour. This leads to pointing out additional terms which contribute to a more actual evaluation of the energy release rate components.

2. Laminate modelisation

With reference to Fig. 1, a two-layer plate is analysed in which the layers are treated as plates in the context of a Reissner-Mindlin type of kinematics. Under the assumption of cylindrical bending (or plane strain in the $x-y$ plane), the adhesion between layers is modelled by means of a linear interface the constitutive law of which involves displacement jumps between the upper and lower layers in the x and y directions only, thus excluding mode III deformation at the interface. The layers are assumed to be homogeneous, orthotropic and linearly elastic and contain a plane crack with its edge aligned with the principal axis of orthotropy z, which is assumed to advance in the direction of the in-plane orthotropy axis x.

The interlaminar tangential and normal stresses σ_{xy} and σ_{yy} at the interface between layers can be expressed as a linear function of the displacement jumps between layers at the interface

$$\begin{Bmatrix} \sigma_{yy} \\ \sigma_{xy} \end{Bmatrix} = \frac{1}{B}\begin{bmatrix} k_v & 0 \\ 0 & k_h \end{bmatrix}\begin{Bmatrix} \Delta w \\ \Delta u \end{Bmatrix}, \tag{1}$$

where $k_h, \Delta u$ and $k_v, \Delta w$ are the elastic stiffnesses of the springs and the relative displacements at the interface in the longitudinal (x) and transversal (y) direction, respectively.

The energy release rate mode components can be calculated in the realm of the linear elastic fracture mechanics (LEFM) through the strain energy per unit surface stored in the interface at the crack tip. In fact, if the stiffnesses of the interlaminar springs approach infinity, the continuity of the displacements at the interface is assured (i.e.Δu and Δw tend to zero) while interlaminar stresses become singular at the crack tip, and the mode components of the energy release rate can be evaluated in a natural way by means of the energy argumentation at the crack tip described in the next paragraphs.

The mode components G_{I} and G_{II} of energy release rate can be calculated by means of the work of interlaminar stresses σ_{yy} and σ_{yx}, in the limit when $k_h, k_v \to \infty$, through the displacement jumps Δw and Δu, respectively, for a virtual crack extension δa (for more details

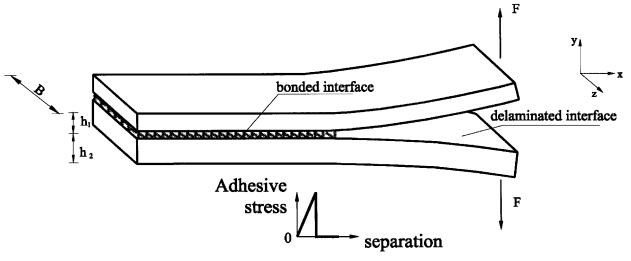

Fig. 1. Scheme of a two-layer plate with a linear interface model.

see [13]). Therefore, for the aliquots of the fracture energy in the opening and in the sliding directions, under the assumption that the mode I component G_{I} corresponds to opening transversal relative displacements at the crack tip (i.e. $\Delta w > 0$), the expressions are found to be

$$G_{\mathrm{I}} = \begin{cases} \frac{1}{B} \lim\limits_{\substack{k_v\to\infty \\ k_h\to\infty}} \frac{1}{2} k_v \Delta w^2, & \text{if } \Delta w > 0 \\ 0, & \text{if } \Delta w \leqslant 0, \end{cases}$$

$$G_{\mathrm{II}} = \frac{1}{B} \lim_{\substack{k_v\to\infty \\ k_h\to\infty}} \frac{1}{2} k_h \Delta u^2, \tag{2}$$

where the subscript I, II denote mode I, II components and Δu andΔw are taken at the delamination tip.

3. Solution of the governing equations

The relevant governing equations will be formulated for the two-layer plate model shown in Fig. 2. The thickness of the upper and lower layers is h_1 and h_2, respectively, and cylindrical bending ($\varepsilon_z = 0$) conditions and clamped end conditions are assumed. The local layer co-ordinate system for each layer is chosen so that the $x-z$ plane coincides with the midplane of the corresponding layer. The layers have the Young modulus E_i along the x axis and Poisson's ratios v_{xzi}, v_{zxi} along the $x-z$ and $z-x$ directions; we denote by $D_i = E_i B h_i^3/[12(1 - v_{xzi}v_{zxi})]$ and $A_i = E_i B h_i/(1 - v_{xzi}v_{zxi})$ the bending and axial stiffness of the ith lamina ($i = 1, 2$), where B is the width of the plate. Isotropic properties can be taken into account setting $v_{xzi} = v_{zxi}$.

Moreover, the shear deformability of the plate is accounted for by introducing the shear stiffness parameters $A_i^* = K_i G_i B h_i$ of the ith layer, where G_i and K_i are the shear modulus and the shear correction factor (see [14] for models to evaluate K_i) of the ith layer, respectively. The following kinematics are used for the ith layer:

$$U_i(x,y) = u_i(x) + y \cdot \psi_i(x),$$
$$W_i(x,y) = w_i(x), \tag{3}$$

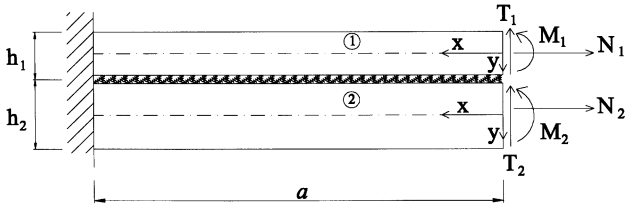

Fig. 2. Geometry and loading configuration for a two-layer plate system.

where the $U_i(x,y)$ in-plane and the $W_i(x,y)$ transverse displacements of the ith layer are expressed as functions of the corresponding midsurface in-plane and transverse displacements $u_i(x)$ and $w_i(x)$, respectively, and of the section rotation $\psi_i(x)$. Note that the components $U_i(x,y)$ and $W_i(x,y)$ are positive when directed as the co-ordinate axes. In what follows the prime denotes the derivative with respect to the x co-ordinate.

The total potential energy of the plate can be expressed in terms of the generalized displacements $u_i(x), w_i(x)$ and $\psi_i(x)$

$$\begin{aligned} &\Pi(u_1, u_2, w_1, w_2, \psi_1, \psi_2) \\ &\quad = \frac{1}{2}\int_0^a \Big[D_1\psi_1'^2 + D_2\psi_2'^2 + A_1^*(\psi_1 + w_1')^2 \\ &\qquad + A_1^*(\psi_2 + w_2')^2 + A_1 u_1'^2 + A_2 u_2'^2\Big]\,\mathrm{d}x \\ &\qquad + \frac{1}{2}\int_0^a (k_h\Delta u^2 + k_v\Delta w^2)\,\mathrm{d}x + N_1 u_1(0) + M_1\psi_1(0) \\ &\qquad + T_1 w_1(0) + N_2 u_2(0) + M_2\psi_2(0) + T_2 w_2(0), \end{aligned} \tag{4}$$

where Δu and Δw are the relative displacements at the interface

$$\Delta w(x) = w_2(x) - w_1(x),$$

$$\Delta u(x) = u_1(x) + \frac{h_1}{2}\psi_1(x) - \left[u_2(x) - \frac{h_2}{2}\psi_2(x)\right], \tag{5}$$

and a is the bonded length of the two-layer plate shown in Fig. 2.

The above formulation can be seen as a stationary problem in which the constraints $\Delta u = 0$, $\Delta w = 0$ for $0 < x < a$ are introduced by means of the penalty coefficients k_h, k_v.

The stationary condition of the total potential energy leads to the following equilibrium equations and natural boundary conditions:

$$\begin{cases} D_1\psi_1'' - A_1^*(\psi_1 + w_1') - k_h\Delta u\frac{h_1}{2} = 0, \\ D_2\psi_2'' - A_2^*(\psi_2 + w_2') - k_h\Delta u\frac{h_2}{2} = 0, \\ A_1^*(\psi_1' + w_1'') + k_v\Delta w = 0, \\ A_2^*(\psi_2' + w_2'') - k_v\Delta w = 0 \\ A_1 u_1'' - k_h\Delta u = 0, \\ A_2 u_2'' + k_h\Delta u = 0, \end{cases} \quad \begin{cases} A_1 u_1'(0) - N_1 = 0, \\ A_2 u_2'(0) - N_2 = 0, \\ A_1^*(\psi_1 + w_1')(0) - T_1 = 0, \\ A_2^*(\psi_2 + w_2')(0) - T_2 = 0, \\ D_1\psi_1'(0) - M_1 = 0, \\ D_2\psi_2'(0) - M_2 = 0. \end{cases} \tag{6}$$

The solution to problem Eq. (6), under the condition that the penalty parameters approach infinity, depends on the boundary conditions at the end of the uncracked plate (i.e. at $x = a$). In fact, the condition of zero relative sliding displacements at the interface does not lead to a zero relative rotation $\psi_1 - \psi_2$ between the layers of the two-layer plate, because of shear deformations (it is assured that only the derivative of the relative transverse displacement $\mathrm{d}\Delta w/\mathrm{d}x$ vanishes). Thus, the two-layer plate cannot be modelled as an equivalent single layer as

in the context of the classical plate theory, because transverse strains are discontinuous at the layer interface due to the non-zero relative section rotation $\psi_1 - \psi_2$.

The energy release rate evaluation depends on the a/h_i ratio; if we assume that this ratio is much greater than unity, the solution is practically unaffected by the essential boundary conditions (i.e. at $x = a$). Under this assumption the proposed model can be applied in the context of a local analysis (i.e. for a plate segment in the neighborhood of the delamination tip) for a general delamination problem once a global analysis is performed to calculate stress resultants acting at cross-sections near the crack tip (Fig. 3)

It is worth mentioning (the details can be found in [13]) that if a Kirchhoff–Love kind of kinematics for the layers were adopted, stresses and deformations at a finite distance from the crack tip do not affect the local solution. Moreover, shear stresses do not contribute to energy release rate computation and thus their fracture effects are neglected; they affect only the stress field at the crack tip.

The same kind of assumption is needed to perform the analysis made by Schapery and Davidson [6] or Suo and Hutchinson [7] in plate problems. In these works, in fact, the problem of the decomposition of the energy release rate is obtained by removing the beam-plate kinematics assumptions, utilised at first to compute the total fracture energy, in the zone containing the delamination edge and thus invoking continuum analysis to solve the problem in the geometry of a semi-infinite crack. The decomposition is so exact for a problem of an infinite cracked plate. In order to apply these results to real plate problems the lengths of the segments of the plate ahead and behind the delamination tip must be assumed sufficiently greater than the transverse thickness of the plate, but small enough to have no significant variations in the applied loads.

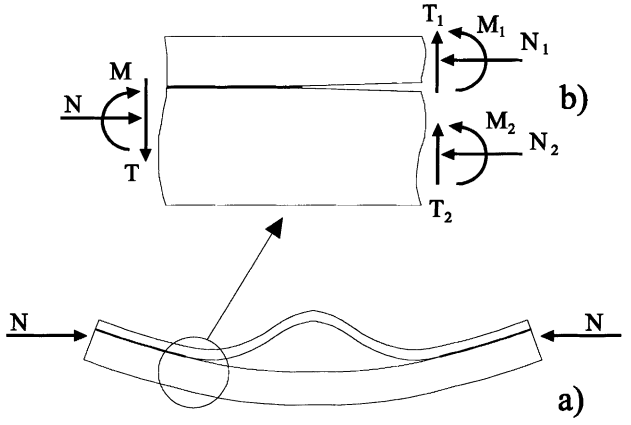

Fig. 3. Example of real plate delamination problems: (a) global analysis, (b) local analysis.

System (6) can be reduced to an algebraic eigenvalues problem $\boldsymbol{Au} = \lambda \boldsymbol{u}$ if we reduce it to the form $\boldsymbol{y}' = \boldsymbol{Ay}$. If we set $\boldsymbol{y} = \{u_1, u_1', u_2, u_2', w_1, w_1', w_2, w_2', \psi_1, \psi_1', \psi_2, \psi_2'\}^{\mathrm{T}}$, $\boldsymbol{A}$ assumes the following form:

$$\boldsymbol{A} = \begin{bmatrix}
0 & 1 & 0 & 0 & 0 & 0 & 0 & 0 & 0 & 0 & 0 & 0 \\
\frac{k_h}{A_1} & 0 & -\frac{k_h}{A_1} & 0 & 0 & 0 & 0 & 0 & \frac{k_h h_1}{2A_1} & 0 & \frac{k_h h_2}{2A_2} & 0 \\
0 & 0 & 0 & 1 & 0 & 0 & 0 & 0 & 0 & 0 & 0 & 0 \\
-\frac{k_h}{A_2} & 0 & \frac{k_h}{A_2} & 0 & 0 & 0 & 0 & 0 & -\frac{k_h h_1}{2A_2} & 0 & -\frac{k_h h_2}{2A_2} & 0 \\
0 & 0 & 0 & 0 & 0 & 1 & 0 & 0 & 0 & 0 & 0 & 0 \\
0 & 0 & 0 & 0 & \frac{k_v}{A_1^*} & 0 & -\frac{k_v}{A_2^*} & 0 & 0 & -1 & 0 & 0 \\
0 & 0 & 0 & 0 & 0 & 0 & 0 & 1 & 0 & 0 & 0 & 0 \\
0 & 0 & 0 & 0 & -\frac{k_v}{A_2^*} & 0 & \frac{k_v}{A_2^*} & 0 & 0 & 0 & 0 & -1 \\
0 & 0 & 0 & 0 & 0 & 0 & 0 & 0 & 0 & 1 & 0 & 0 \\
\frac{k_h h_1}{2D_1} & 0 & -\frac{k_h h_1}{2D_1} & 0 & 0 & \frac{A_1^*}{D_1} & 0 & 0 & \frac{A_1^*}{D_1} + \frac{k_h h_1^2}{4D_1} & 0 & \frac{k_h h_1 h_2}{4D_1} & 0 \\
0 & 0 & 0 & 0 & 0 & 0 & 0 & 0 & 0 & 0 & 0 & 1 \\
\frac{k_h h_2}{2D_2} & 0 & -\frac{k_h h_2}{2D_2} & 0 & 0 & 0 & 0 & \frac{A_2^*}{D_2} & \frac{k_h h_1 h_2}{4D_2} & 0 & \frac{A_2^*}{D_2} + \frac{k_h h_2^2}{4D_2} & 0
\end{bmatrix}.$$

The eigenvalue matrix, for sufficiently high values of the penalty parameters k_h and k_v, takes the form: $\Lambda = \mathrm{diag}\{\alpha, -\alpha, \beta, -\beta, \gamma, -\gamma, 0, 0, 0, 0, 0, 0\}$, where α, β, γ are real numbers. The solution to the problem at hand can be found by a linear combination of the particular integrals: $\boldsymbol{y} = \sum_{j=1}^{12} c_i \boldsymbol{u_i} e^{\lambda_i x}$: to do this we need to solve the eigensystem of $\boldsymbol{A}$. If we suppose that the plate has high a/h_i ratios the eigensolutions with a positive real part can be excluded from the solution. On the other hand, if the above-mentioned assumption is not satisfied, all boundary conditions noticeably affect the crack tip solution.

The boundary condition can be expressed in the form $\boldsymbol{Uc} = \boldsymbol{f}$, where

$$\boldsymbol{f} = \left\{0, \frac{N_1}{A_1}, 0, \frac{N_2}{A_2}, 0, \frac{T_1}{A_1^*}, 0, \frac{T_2}{A_2^*}, 0, \frac{M_1}{D_1}, 0, \frac{M_2}{D_2}\right\}^{\mathrm{T}},$$

$\boldsymbol{c}$ is the vector the components of which are the coefficients c_i of the linear combination of particular solutions and the boundary condition matrix $\boldsymbol{U}$ is

$$\boldsymbol{U} = \begin{bmatrix}
u_{1,1}e^{\lambda_1 a} & \dots & u_{1,6}e^{\lambda_6 a} & u_{1,7} & \dots & u_{1,12}a^5 \\
u_{2,1} & \dots & u_{2,6} & u_{2,7} & \dots & 0 \\
u_{3,1}e^{\lambda_1 a} & \dots & u_{3,6}e^{\lambda_6 a} & u_{3,7} & \dots & u_{3,12}a^5 \\
u_{4,1} & \dots & u_{4,6} & u_{4,7} & \dots & 0 \\
u_{5,1}e^{\lambda_1 a} & \dots & u_{5,6}e^{\lambda_6 a} & u_{5,7} & \dots & u_{5,12}a^5 \\
u_{6,1} + u_{9,1} & \dots & u_{6,6} + u_{9,6} & u_{6,7} + u_{9,7} & \dots & 0 \\
u_{7,1}e^{\lambda_1 a} & \dots & u_{7,6}e^{\lambda_6 a} & u_{7,7} & \dots & u_{7,12}a^5 \\
u_{8,1} + u_{11,1} & \dots & u_{8,6} + u_{11,6} & u_{8,7} + u_{11,7} & \dots & 0 \\
u_{9,1}e^{\lambda_1 a} & \dots & u_{9,6}e^{\lambda_6 a} & u_{9,7} & \dots & u_{9,12}a^5 \\
u_{10,1} & \dots & u_{10,6}e^{\lambda_6 a} & u_{10,7} & \dots & 0 \\
u_{11,1}e^{\lambda_1 a} & \dots & u_{11,6}e^{\lambda_6 a} & u_{11,7} & \dots & u_{11,12}a^5 \\
u_{12,1} & \dots & u_{12,6} & u_{12,12} & \dots & 0
\end{bmatrix},$$

where $u_{i,j}$ is the ith component of the jth eigenvector.

Fig. 4 illustrates the behaviour of the interlaminar stress field for a double cantilever scheme with an off-centre crack $(h_1/h_2 = 0.5)$. The essential geometrical and mechanical parameters are: $E_1 = 70.000$ MPa,

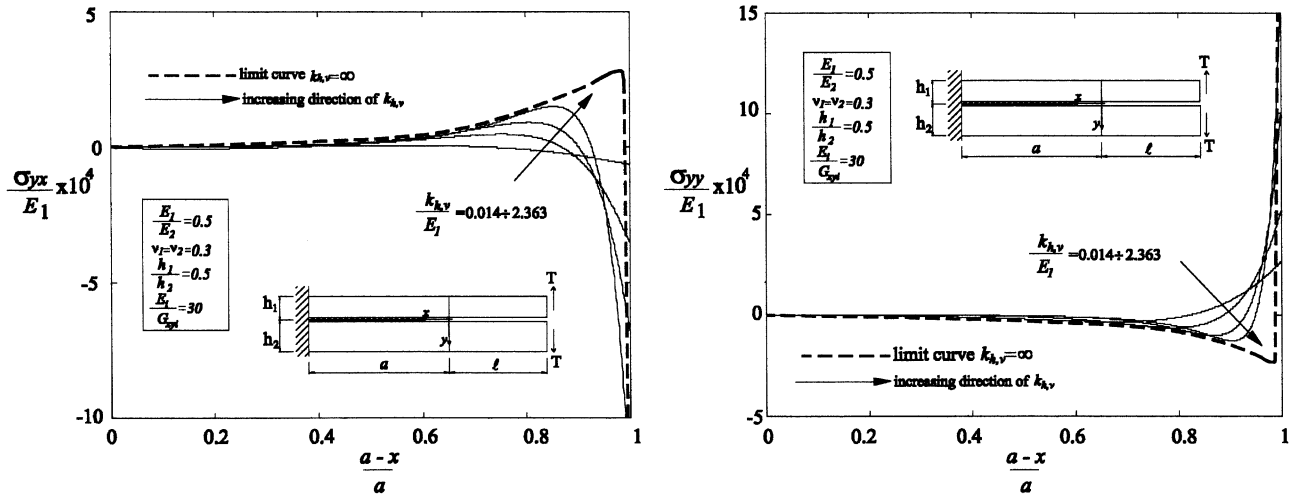

Fig. 4. Shear and normal interlaminar stresses behaviour for increasing values of the penalty parameters k_v, k_h.

$h_1 = 1$ mm, $l = 10$ mm, $a = 20$ mm, $T_1 - T_2 = 100$ N, $B = 10$ mm. The mechanical parameters are chosen to be representative of a typical Aramid fibre epoxy composite for the upper layer and of a carbon fibre epoxy for the lower layer. Shear and normal interlaminar stresses are plotted (unbroken curves in Fig. 4) for different values of the dimensionless interface stiffness parameters $k_{h,v}/E_1$ ranging in geometric progression from 0.014 to 2.363. It is of some importance to notice that the interlaminar stresses, as interface stiffnesses approach infinity, tend to a non-zero function of an exponential kind which has a singularity at the crack tip (dashed curves in Fig. 4). This behaviour is due to the kinds of kinematics adopted: as a matter of fact, a global self-equilibrating loading system does not lead to a zero stress field in the two-layer plate at a finite distance from the crack tip, but it decays with an exponential-like behaviour as the distance from the crack tip increases.

In Fig. 5 the convergence of the energy release rate components to their limit values (i.e. $k_h, k_v, \to \infty$) as evaluated from Eq. (2), is investigated. For convenience a logarithmic scale (base 10) is used for the horizontal axis. In this figure a comparison is made between the total energy release rate as calculated from the classical plate theory (CPT) G_{CPT}, the total energy release rate $\bar{G}_{\mathrm{CPT}}$ corrected to account for shear deformation

$$\bar{G}_{\mathrm{CPT}} = \frac{1}{2B}\left(\frac{M_1^2}{D_1} + \frac{M_2^2}{D_2} + \frac{T_1^2}{A_1^*} + \frac{T_2^2}{A_2^*}\right) \tag{7}$$

and the total energy release rate G as computed by means of the proposed model.

Moreover, a comparison between energy release rate mode components as calculated by utilising the Kirchhoff plate models for the layers in conjunction with a linear interface model [13] $G_{\mathrm{I}}^{\mathrm{K}}, G_{\mathrm{II}}^{\mathrm{K}}$ and by using the proposed model $G_{\mathrm{I}}, G_{\mathrm{II}}$, is made. It is worth mentioning that the sum of $G_{\mathrm{I}}^{\mathrm{K}}, G_{\mathrm{I}}^{\mathrm{K}}$ is equal to the global energy release rate obtained by using the classical plate theory G_{CPT}. Note that in Fig. 5 the values for $G_{\mathrm{I}}, G_{\mathrm{II}}$ are plotted in the penalty procedure as k_v and k_h approach infinity with the same velocity.

At first it can be noted that the total energy release rate G predicted by the proposed model is more than in the Kirchhoff one due to normal/shear stress coupling effects. As can be noted in Fig. 5, the difference between G_{I} and $G_{\mathrm{I}}^{\mathrm{K}}$ is more notable than that between G_{II} and $G_{\mathrm{II}}^{\mathrm{K}}$: this arises from the strong influence of the additional normal/shear stress coupling terms on mode I energy release rate.

As far as the Kirchhoff model is employed to model layers, the global fracture energy G_{CPT}, and thus its mode components $G_{\mathrm{I}}^{\mathrm{K}}, G_{\mathrm{II}}^{\mathrm{K}}$, are noticeably underestimated (the relative error $(G - G_{\mathrm{CPT}})/G(\%)$ is about the 25%). This is also true if the influence of shear deformation is

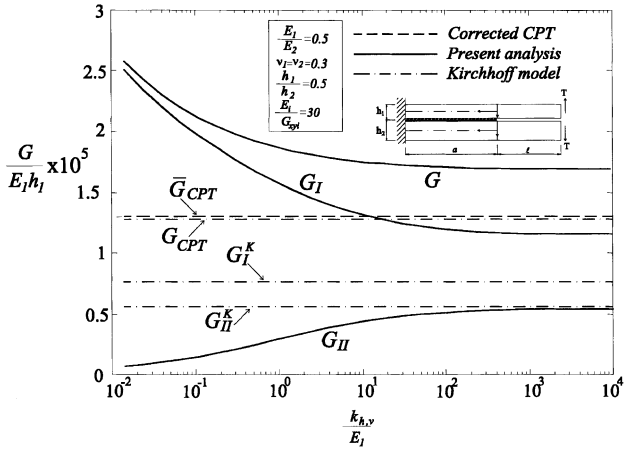

Fig. 5. Energy release rates evaluation for different layered plate model.

accounted for (the relative error $(G-\bar{G}_{\mathrm{CPT}})/G(\%)$ is about the 22.4%). This phenomenon can be attributed to the normal/shear stress coupling effects arising in energy release rate evaluation.

Moreover, it is worth observing that the hypothesis that two opposite moments lead to activating only mode I component made in [9] is approximate.

Interesting features of the energy release rate modelling can be captured by referring to the orders of singularity of interlaminar stresses at the crack tip as the penalty parameters approach infinity:

$$\sigma^{M,N}_{yy,yx} = \mathrm{O}(k^{1/2}_{h,v}) + \mathrm{o}(k^{1/2}_{h,v}), \quad k_{h,v} \to \infty,$$

$$\sigma^{\mathrm{T}}_{yy,yx} = \mathrm{O}(k^{1/2}_{h,v}) + \mathrm{o}(k^{1/2}_{h,v}), \quad k_{h,v} \to \infty,$$

where $\sigma^{M,N}_{yy,yx}$ and $\sigma^{\mathrm{T}}_{yy,yx}$ are the interlaminar stresses arising from axial/bending (i.e. N_1, N_2, M_1, M_2) and shear loading condition (i.e. T_1, T_2), respectively, $\mathrm{O}(k^{1/2}_{h,v})$ is referred to terms of $k^{1/2}_{h,v}$ order and $\mathrm{o}(k^{1/2}_{h,v})$ is referred to terms which go to infinity slower than $k^{1/2}_{h,v}$ as $k^{1/2}_{h,v} \to \infty$. The previous asymptotic expansions of interlaminar stresses, show that contrary to the case in which the Kirchhoff plate theory is used to model each layer and the first term in $\sigma^{\mathrm{T}}_{yy,yx}$ vanishes (see [13]), interlaminar shear stresses give a non-zero contribution to energy release rate. This can be proved by looking at Eq. (2) and considering that the order of displacement jumps $\Delta u, \Delta w$ are $\mathrm{O}(k^{-1/2}_{h,v})$.

4. J-integral argumentation

The energy release rate in a cracked laminate, can be calculated with the aid of the J-integral concept. In this paragraph the previous results will be interpreted by utilising the J-integral approach. In the context of the classical plate theory the uncracked plate can be considered as a single layer. In an approximate way the effect of shear deformation can be evaluated assuming the presence of shear stresses as required from equilibrium condition. If we assume for C a rectangle path surrounding the crack tip with two vertical lines across the layers (see path ABCDEF in Fig. 6) we have:

$$\begin{aligned} J &= \oint_C \left(-\frac{1}{2}\sigma_{ij}\varepsilon_{ij}\,\mathrm{d}y - \sigma_{ij}n_j\frac{\partial u_i}{\partial x}\,\mathrm{d}s \right) \\ &= \oint_C \left[-\frac{1}{2}\left(\frac{1-\upsilon_{zx}\upsilon_{xz}}{E_x}\sigma^2_{xx} + \frac{\sigma^2_{xy}}{G_{xy}} \right) \right. \\ &\qquad \left. + \sigma_{xx}\frac{\partial u}{\partial x} + \sigma_{xy}\frac{\partial w}{\partial x} \right] \mathrm{d}y \\ &= \oint_C \frac{1}{2}\left(\frac{1-\upsilon_{zx}\upsilon_{xz}}{E_x}\sigma^2_{xx} + \frac{\sigma^2_{xy}}{G_{xy}} \right) \mathrm{d}y - \oint_C \sigma_{xy}\frac{\partial u}{\partial y}\,\mathrm{d}y, \end{aligned} \quad (8)$$

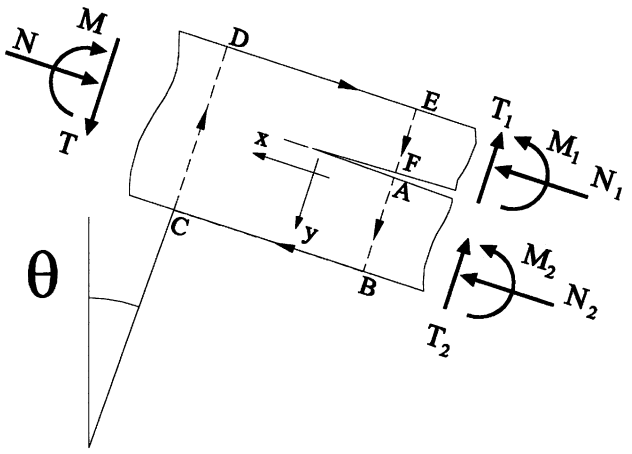

Fig. 6. J-integral path around the crack tip.

where it is assumed that along the vertical segments of C, taken sufficiently distant from the delamination front, the plate theory assumption $\sigma_{yy} = 0$ is satisfied.

In the context of the Reissner–Mindlin kinematics (or the first order shear deformation plate theory (FSDT)) utilised for the whole laminate thus assuming the transverse shear strains γ_{xy} continuous across the interface, from the first term in Eq. (8) $(1-\nu_{xz}\nu_{zx})\sigma^2_{xx}/E_x$, we can recover the global fracture energy G_{CPT} which is the same of that calculated from the CPT

$$G_{\mathrm{CPT}} = G^{\mathrm{EF-AB}}_{\mathrm{CPT}} + G^{\mathrm{CD}}_{\mathrm{CPT}}, \quad (9)$$

where

$$G^{\mathrm{EF-AB}}_{\mathrm{CPT}} = \frac{1}{2B}\left(\frac{N_1^2}{A_1} + \frac{N_2^2}{A_2} + \frac{M_1^2}{D_1} + \frac{M_2^2}{D_2} \right),$$

$$\begin{aligned} G^{\mathrm{CD}}_{\mathrm{CPT}} = &-\frac{1}{2B} \\ &\left[\left\{ \frac{E_2 h_2}{1-\nu_{zx2}\nu_{xz2}}(12M^2 - 12h_1MN + (3h_1^2 + h_2^2)N^2) \right. \right. \\ &\quad \left. + \frac{E_1 h_1}{1-\nu_{zx1}\nu_{xz1}}(12M^2 + 12h_2MN + (h_1^2 + 3h_2^2)N^2) \right\} \Big/ \\ &\left\{ B\left[\frac{E_1^2 h_1^4}{(1-\nu_{zx1}\nu_{xz1})^2} + \frac{E_2^2 h_2^4}{(1-\nu_{zx2}\nu_{xz2})^2} \right. \right. \\ &\quad \left. \left. + 2\frac{E_1 h_1}{1-\nu_{zx1}\nu_{xz1}}\frac{E_2 h_2}{1-\nu_{zx1}\nu_{xz1}}(2h_1^2 + 3h_1h_2 + 2h_2^2) \right] \right\} \Big]. \end{aligned}$$

The first and second terms at the right-hand side of Eq. (9) are the bending and extensional energies stored in the plate per unit of length ahead and behind the delamination tip, respectively. The integration path C is taken at a small distance from the crack tip, so that energy release rate is a function only of forces and moments acting on the boundary of the element containing the crack tip.

On the other hand, the amount of energy arising from the second term σ_{xy}^2/G_{xy} in Eq. (8) is the approximate shear correction ΔG_{SC} to energy release rate

$$\Delta G_{SC} = \frac{1}{2B}\left(\frac{T_1^2}{A_1^*} + \frac{T_2^2}{A_2^*} - \frac{T^2}{A_1^* + A_2^*}\right). \tag{10}$$

To obtain the previous term we have assumed that transverse shear strains γ_{xy} are continuous across the interface. This term can be also obtained in the context of the classical plate theory by considering the shear stresses arising from equilibrium condition. For this reason this term is referred to as approximate shear correction energy. It can be noted that until now bending, axial and transverse shear stress resultants give rise to an orthogonal energetic system in energy release rate calculation (i.e. no coupling terms between M_i, N_i and T_i arise in energy release rate).

The remaining term $\sigma_{xy}\partial u/\partial y$ makes no contribution in the context of the Kirchhoff–Love or of the Reissner–Mindlin plate theory due to the assumption of the continuity of the derivative of the axial displacement with respect to the thickness co-ordinate $\partial u/\partial y$ across the interface. In fact, from equilibrium requirement along the y direction and considering that the crack tip element exhibits a rigid rotation θ see Fig. 6), the integral along the path C of the above discussed term is zero

$$-\oint_C \sigma_{xy}\frac{\partial u}{\partial y}\,\mathrm{d}y = -\theta\oint_C \sigma_{xy}\,\mathrm{d}y = \frac{\theta}{B}(-T_1 - T_2 + T) = 0.$$

If the present interface model is adopted, instead, this term becomes responsible for normal/shear stress interaction contribution to energy release rate. This term, in fact, is due to a non-zero relative rotation between layers which, depending on natural boundary conditions at the crack tip, produces normal/shear stress interaction. We can refer to this aliquot of energy release rate also as a shear rotation energy term. As a matter of fact, in our model the constraint condition imposed as spring stiffnesses approach infinity, assures only displacement continuity. Thus, the contribution of the term involving shear stresses and section rotations becomes

$$-\oint_C \sigma_{xy}\frac{\partial u}{\partial y}\,\mathrm{d}y = -\psi_1\frac{T_1 - \bar{T}_1}{B} - \psi_2\frac{T_2 - \bar{T}_2}{B}, \tag{11}$$

where $\bar{T}_1, \bar{T}_2$ are shear forces acting on the upper and lower section behind the delamination tip (see Fig. 7). Moreover, in the context of the interface model here introduced, in order to calculate the effective contributions of the first and second terms in Eq. (10), the actual strain field at the crack tip should be taken into account which considers the possibility of a discontinuity of section rotation across the interface.

Definitively, the global energy release rate can be put in the following form:

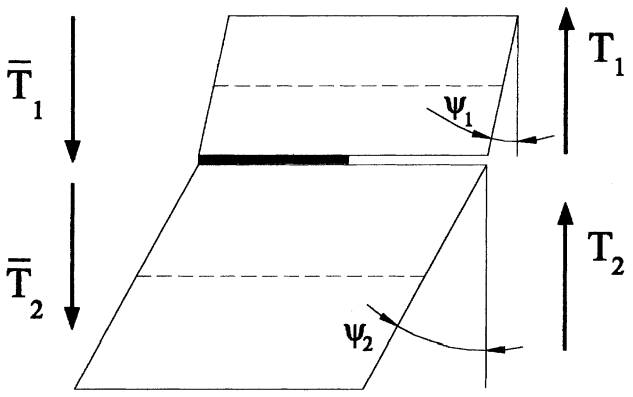

Fig. 7. Relative rotation of sections at the crack tip.

$$G_T = G_{CPT} + \Delta G_{SC} + \Delta G_{N/S}, \tag{12}$$

where the first term is the energy release rate as calculated by means of the classical plate theory, the second term is the approximate shear fracture energy and the third is the normal/shear stress interaction fracture energy. Therefore the influence of shear cannot be circumscribed only to the standard terms T_i^2/BA_i^*, (see [9]) but other terms must also be accounted for arising from the stress interaction, which can have an important effect on the energy release rate value, especially for laminates with a low shear to bending stiffness ratio.

5. Application to delamination specimens

In this section we will consider some examples of delamination specimens in mode I, mode II and mixed modes, commonly used to determine the interlaminar fracture toughness of laminated composites. The influence of shear stresses on energy release rate evaluation will be evidenced in the context of the model here presented.

5.1. Mode I testing

The most common scheme adopted for studying mode I crack propagation, is the double cantilever beam (DCB) configuration.

With reference to this simple scheme ($h_1 = h_2 = h, A_1 = A_2 = A, A_1^* = A_2^* = A^*$ and $D_1 = D_2 = D$) and in the case of the symmetrical loading condition (see Fig. 8) it is possible to get an analytical solution. The relevant governing equations, after some manipulations, can be written as

$$\begin{aligned} &A^*(\psi_1' + w_1'') - 2k_v w_1 = 0,\\ &A^*(\psi_1 + w_1') - D\psi_1'' = 0 \end{aligned} \tag{13}$$

with the following boundary conditions:

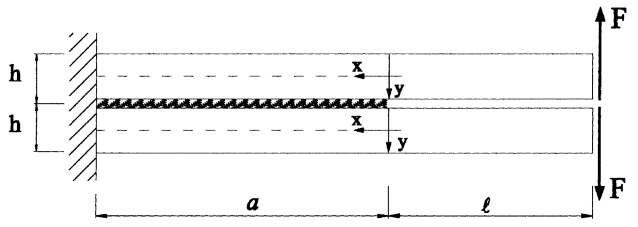

Fig. 8. Geometry and loading mode for the two-layer symmetrical scheme.

$$w_1(a)=0,\psi_1(a)=0,\quad D\psi_1'(0)=M,$$
$$A^*(\psi_1+w_1')(0)=T, \tag{14}$$

where $F=T$ and $M=Tl$. The above boundary value problem can be solved by reducing the system of second order linear differential equations to homogeneous system of linear differential equations of the first order. Assuming $\boldsymbol{y}=\{w_1,w_1',\psi_1,\psi_1'\}^{\mathrm{T}}$, the linear operator A takes the configuration

$$\boldsymbol{A}=\begin{bmatrix}0 & 1 & 0 & 0\\ \frac{2k_v}{A^*} & 0 & 0 & -1\\ 0 & 0 & 0 & 1\\ 0 & \frac{A^*}{D} & \frac{A^*}{D} & 0\end{bmatrix}, \tag{15}$$

the solution has the form $\boldsymbol{y}=\sum_{j=1}^{4}c_i\boldsymbol{u_i}e^{\lambda_i x}$ and the boundary conditions can be put in the form $\boldsymbol{Uc}=\boldsymbol{f}$, where

$$\boldsymbol{U}=\begin{bmatrix}u_{1,1}e^{\lambda_1 a} & u_{1,2}e^{\lambda_2 a} & u_{1,3}e^{\lambda_3 a} & u_{1,4}e^{\lambda_4 a}\\ u_{2,1}+u_{3,1} & u_{2,2}+u_{3,2} & u_{2,3}+u_{3,3} & u_{2,4}+u_{3,4}\\ u_{3,1}e^{\lambda_1 a} & u_{3,2}e^{\lambda_2 a} & u_{3,3}e^{\lambda_3 a} & u_{3,4}e^{\lambda_4 a}\\ u_{4,1} & u_{4,2} & u_{4,3} & u_{4,4}\end{bmatrix}, \tag{16}$$

while $\boldsymbol{f}=\{0,T/A^*,0,M/D\}$.

The eigenvalues of the matrix $\boldsymbol{A}$ can be expressed as $\Lambda=\mathrm{diag}\{\alpha,-\alpha,\beta,-\beta\}$ where

$$\alpha=\sqrt{\frac{Dk_v-\sqrt{Dk_v(Dk_v-2A^{*2})}}{A^*D}}\quad\text{and}$$
$$\beta=\sqrt{\frac{Dk_v+\sqrt{Dk_v(Dk_v-2A^{*2})}}{A^*D}}.$$

Since we are interested in the behaviour of the solution as $k_v\to\infty$, we found that

$$\lim_{k_v\to\infty}\alpha=\sqrt{\frac{A^*}{D}}\quad\text{and}\quad\lim_{k_v\to\infty}\beta=\infty.$$

If we suppose that the length of the bonded plate a is much greater than h (i.e. a plate with infinite length) the only meaningful eigenvalues become the negative ones, thus the energy release rate can be computed by utilising only the terms of the solution associated with $-\alpha,-\beta$. If we indicate these two positive eigenvalues with $\lambda_{1,2}$, it is found that the energy release rate becomes (only mode I is involved due to the symmetry of the problem)

$$G_{\mathrm{I}}=\lim_{k_v\to\infty}\frac{1}{2B}k_v\Delta w^2=\lim_{k_v\to\infty}\frac{1}{2B}k_v\left(\sum_{i=1,2}2c_iu_{1i}\right)^2$$
$$=\frac{1}{B}\left(\frac{M}{\sqrt{D}}+\frac{T}{\sqrt{A^*}}\right)^2=\frac{M^2}{DB}+\frac{T^2}{A^*B}+\frac{2MT}{B\sqrt{A^*D}}. \tag{17}$$

From Eq. (17) one can see that two new terms appear in energy release rate expression with respect to the Kirchoff–Love beam-plate model M^2/DB. The first term T^2/BA^* arises from the difference between the strain energy stored (per unit of length) in the plate due to shear stresses ahead and behind the crack tip, while the second one $2MT/B\sqrt{A^*D}$ arises in this case, from stress interaction in the form of bending/shear stress coupling $\Delta G_{\mathrm{B/S}}$.

The same results can be obtained by applying the J-integral to a rectangle path with C-D (see Fig. 6) taken far away the delamination tip (i.e. at a infinite distance from the crack tip). The energy release rate in the context of classical plate theory Eq. (9) is

$$G_{\mathrm{CPT}}=\frac{M^2}{DB}, \tag{18}$$

while the shear correction term Eq. (10) is:

$$\Delta G_{\mathrm{SC}}=\frac{T^2}{A^*B}. \tag{19}$$

As far as the interface model founded on the Mindlin kinematics is concerned, the following is found:

$$\lim_{k_v\to\infty}w_1'(0)=\frac{M}{\sqrt{A^*D}}+\frac{T}{A^*},$$
$$\lim_{k_v\to\infty}\psi_1(0)=-\frac{M}{\sqrt{A^*D}}. \tag{20}$$

Thus, if an end couple is applied, the function w_1' goes to zero for $0<x\leqslant a$, with a discontinuity at $x=0$, while ψ_1 tends toward the function $\psi_1(0)e^{-\sqrt{A^*/D}x}$ (see Fig. 9).

Moreover, in this case interlaminar stresses extinguish along the length of the beam. On the other hand, if a shear force T is only applied, w_1' exhibits similar behaviour, but ψ_1 is identically zero for every x and the interlaminar tension is zero for $0<x\leqslant a$.

If we apply the J-integral technique with the vertical path behind the crack tip so far that we can assume $\psi_1=0$ (i.e. taking these vertical path at $x\gg h$) in the form of Eq. (8), we find

$$J=\int_{-h/2}^{h/2}\left(\frac{1-\upsilon_{xz}^2}{E_x}\sigma_x^2+\frac{\sigma_{xy}^2}{G_{xy}}\right)\mathrm{d}y-2\int_{-h/2}^{h/2}\sigma_{xy}\psi_1(0)\,\mathrm{d}y$$
$$=\frac{M^2}{BD}+\frac{T^2}{BA^*}+2\frac{MT}{B\sqrt{A^*D}}, \tag{21}$$

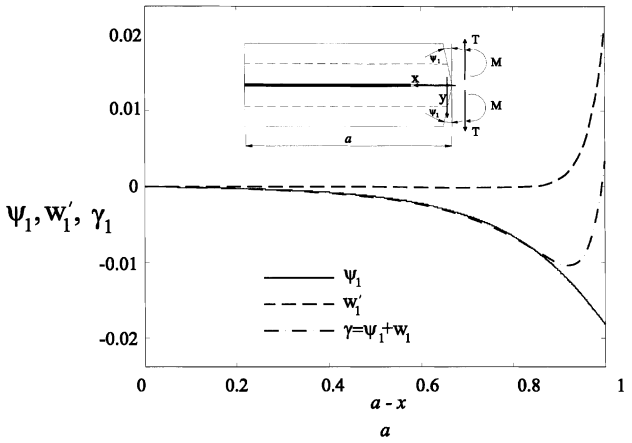

Fig. 9. Behaviour of displacement parameter in the two-layer symmetrical scheme.

where we can see that the coupling term $2MT/B\sqrt{A^*D}$ arises from the discontinuity of the end rotation between the two sections enclosing the crack tip.

Thus the bending/shear fracture energy $\Delta G_{B/N}$ in this case is

$$\Delta G_{B/S} = \frac{2MT}{B\sqrt{A^*D}}. \tag{22}$$

Moreover, to give a better understanding of this behaviour it is useful to evaluate the energy release rate G_I as the derivative of the total potential energy Π with respect to the crack length. The vertical displacement of the point of force application (Fig. 10), as k_v approaches infinity, tends to the limit value

$$w_{DCB} = -\left(\frac{Fl^3}{3D} + \frac{Fl}{A^*} + \frac{Fl^2}{\sqrt{A^*D}}\right) \tag{23}$$

and the energy release rate is given by

$$G_I = -\frac{d\Pi}{Bdl} = \frac{d}{Bdl}(Fw_{DSB}) = \frac{M^2}{DB} + \frac{T^2}{A^*B} + \frac{2MT}{B\sqrt{A^*D}}.$$

In Fig. 11 an investigation on the behaviour of energy release rate is performed, showing a comparison between the results obtained from the complete solution (i.e. without excluding the positive eigenvalues) of the interface model as the a/h ratio increases, and those corresponding to Eq. (17)–(19). The following mechanical, geometrical and loading parameters are used (taken to be representative of a common graphite fibre epoxy composite)

$h = 1$ mm, $\quad E_x = 140.000$ MPa, $\quad l = 10$ mm,

$F = 200$ N, $\quad B = 20$ mm.

We can see that for high values of the a/h ratio, the energy release rate G for $k_v/E_1 \to \infty$ is practically equal to that computed from Eq. (17) and that the cross product term has a significant effect on the energy release rate evaluation. In comparison with the bending energy release rate the shear part is equal to the 5.13% (i.e. the influence of the second term in Eq. (17) T^2/BA^*), while the bending/shear part is equal to the 45.23% (i.e. the influence of the third term in Eq. (17) $2MT/B\sqrt{A^*D}$). When the E/G ratio is relatively high (this is the case of the common laminates) we have to take into account not only the shearing effects but, above all, the coupling effect between the shear force and bending moment. For an isotropic material with $E/G = 2.6$, for instance, the shear term is equal to the 0.27% while the coupling term is equal to 10.26%.

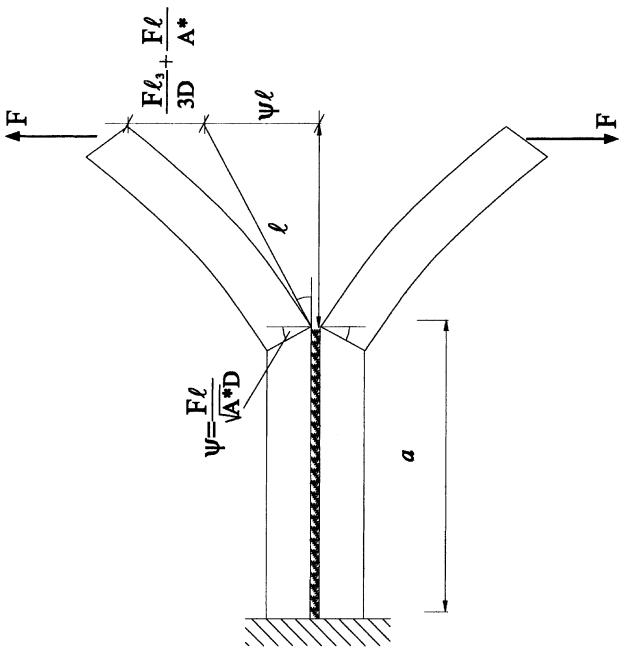

Fig. 10. Deformed configuration of the two-layer symmetrical scheme.

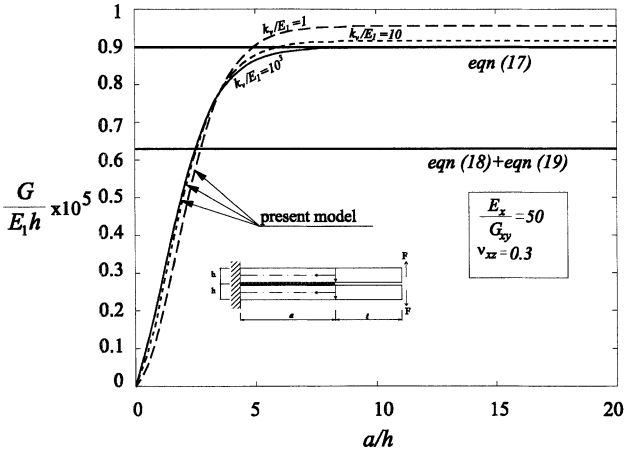

Fig. 11. Energy release rate for various a/h ratios: influence of shear.

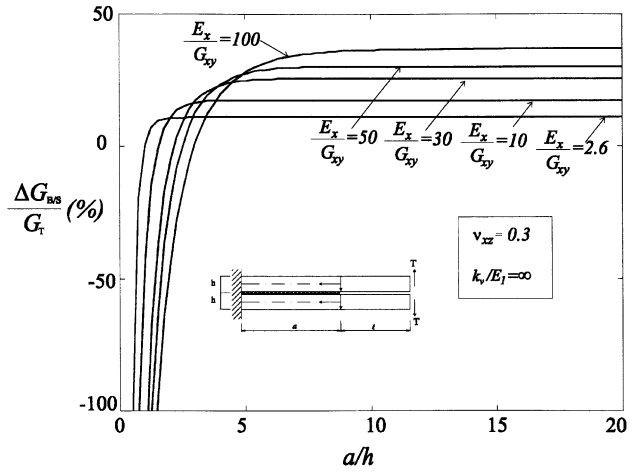

Fig. 12. Relative difference of the energy release rate for various E_x/G_{xy} ratios.

Fig. 12 shows the behaviour of the relative difference $[G_T - (G_{CPT} + G_{SC})]/G_T$ (%) for increasing values of the longitudinal to transverse shear modulus ratio.

This important effect can arise only if an improved beam-plate model that includes the shear deformation effects is used. In fact, if the shear effects are recovered only by equilibrium conditions no coupling effects emerge. In Fig. 13 we can see how the interlaminar normal stresses tend toward a non-null function (i.e. $-\psi_1(0)\sqrt{(A^*/D)}e^{-\sqrt{A^*/D}x}$) with a singularity at the crack tip. This is due to the behaviour of the section rotation function ψ_1.

5.2. Mode II testing

The end loaded split configuration (ELS) is frequently used to evaluate the energy release rate in pure mode II delamination (see Fig. 14).

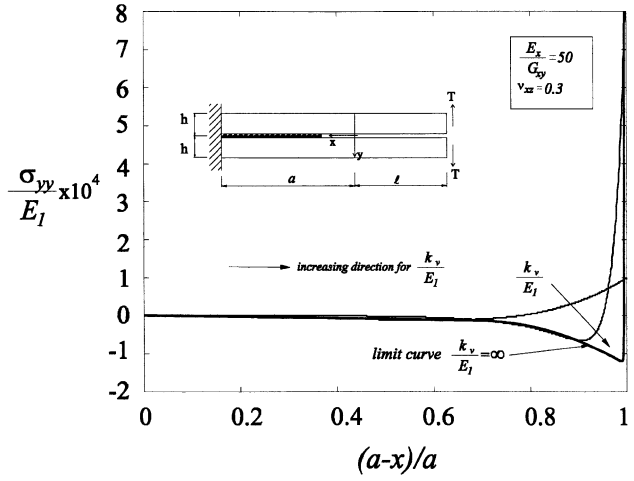

Fig. 13. Interlaminar normal stresses as a function of the interface penalty parameter k_v.

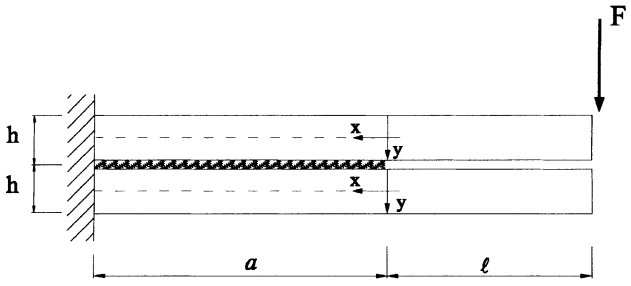

Fig. 14. Mode II delamination scheme (ELS).

Taking into account the particular geometry and loading condition of this example, after some manipulations of Eq. (6) the governing equations of the problem can be cast in the following form:

$$\begin{aligned} &\Delta u'' - \left(\frac{h^2}{2D} + \frac{2}{A}\right)k_h \Delta u - \frac{hT}{D} = 0, \\ &\Delta u(a) = 0, \\ &\Delta u'(0) = \frac{hM}{D_1}, \end{aligned} \tag{24}$$

where $\Delta u = 2u_1 + h\psi_1$, $T = -F/2$ and $M = -Fl/2$.

The solution of (24) takes the form

$$\begin{aligned} \Delta u = {} & \frac{Ahe^{-\alpha\sqrt{k_h}x}(-e^{\alpha a\sqrt{k_h}} + e^{\alpha\sqrt{k_h}x})}{k_h(4D + Ah^2)(1 + e^{2\alpha a\sqrt{k_h}})}[(e^{\alpha a\sqrt{k_h}} + e^{\alpha\sqrt{k_h}x}) \\ & \times 2\alpha\sqrt{k_h}M + 2(e^{\alpha\sqrt{k_h}(a+x)} - 1)T], \end{aligned} \tag{25}$$

where $\alpha^2 = h^2/2D + 2/A$, thus applying Eq. (2) leads to the following:

$$G_{II} = \frac{1}{B}\lim_{k_h\to\infty}\frac{1}{2}k_h\Delta u(0)^2 = \frac{3M^2}{4BD}. \tag{26}$$

As we can note from Eq. (26), shear stresses do not affect the energy release rate value, which is due to the particular geometry and loading condition considered. As a matter of fact, the contribution to the energy release rate is restricted only to that arising from the Classical Plate G_{CPT}, because the shear correction aliquot ΔG_{SC} is zero (see Eq. (10)) and no normal/shear stress interaction is present due to the zero relative rotation between layers (see Eq. 11) being $\psi_1 = \psi_2$ for this antisymmetrical scheme. The uncracked plate of length a as k_h approaches infinity behaves like a unique plate subjected to an end force F and a moment Fl and the global section rotation $\psi = \psi_1 = \psi_2$ governed by the following differential problem:

$$\begin{aligned} &\psi^{IV} - \left(\frac{h^2}{2D} + \frac{2}{A}\right)k_h \quad \psi'' + \frac{2Tk_h}{AD} = 0, \\ &\psi(a) = 0, \quad \psi'(0) = \frac{M}{D}, \\ &\psi''(a) = \frac{T}{D}, \quad \psi'''(0) = \frac{k_h M h^2}{2D^2}, \end{aligned} \tag{27}$$

tends to the parabolic function

$$\psi = \frac{T(x^2 - a^2)}{8D} + \frac{M(x-a)}{4D}$$

(see Fig. 15, the geometrical and mechanical parameters are the same of those used in the mode I test with $F = 400$ N).

Thus, the end point vertical displacement becomes

$$w_{\mathrm{ELS}} = \frac{F(a^3 + 3a^2 l + 3al^2 + 4l^3)}{24D} + \frac{F(a+l)}{2A^*} \tag{28}$$

and the energy release rate is calculated differentiating the total potential energy, resulting

$$G_{\mathrm{II}} = -\frac{\mathrm{d}\Pi}{B\mathrm{d}l} = \frac{\mathrm{d}}{B\mathrm{d}l}\left(\frac{1}{2}Fw_{\mathrm{ELS}}\right) = \frac{3F^2l^2}{16BD} = \frac{3M^2}{4DB}.$$

The behaviour of the interlaminar shear stresses is shown in Fig. 16, where it can be noted that they tend to the constant value $3/2T/Bh$ for $0 < x < a$ and to a singular value at the crack tip to equilibrate the resultant of the normal stresses acting at the cross section containing the crack tip.

5.3. Mixed mode testing

Let us consider the symmetrical two-layer scheme subjected to a general loading system in Fig. 17: it is thus possible to obtain all mixed mode situation by varying loading condition. For example if $F_1 = N_1 = N_2 = 0$ we obtain the asymmetric end loaded split scheme (AELS), or if $N_1 = N_2 = 0$ we obtain the asymmetrically loaded double cantilever beam scheme (ALDCB), both commonly used for the experimental study of mixed mode delamination.

After some manipulations of Eq. (6) we can extract the following differential problem for mode I computation:

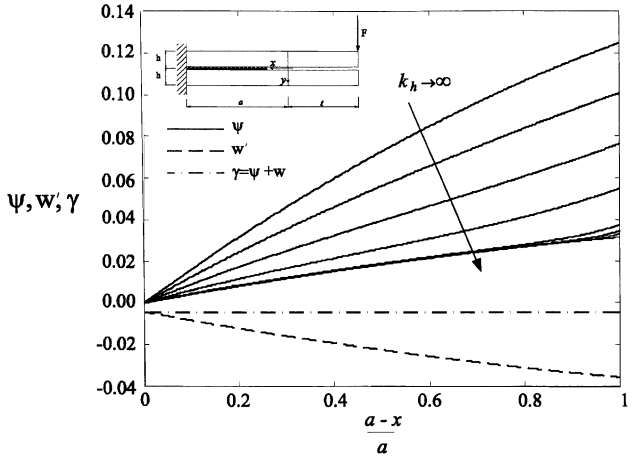

Fig. 15. Behaviour of displacements parameter in the ELS.

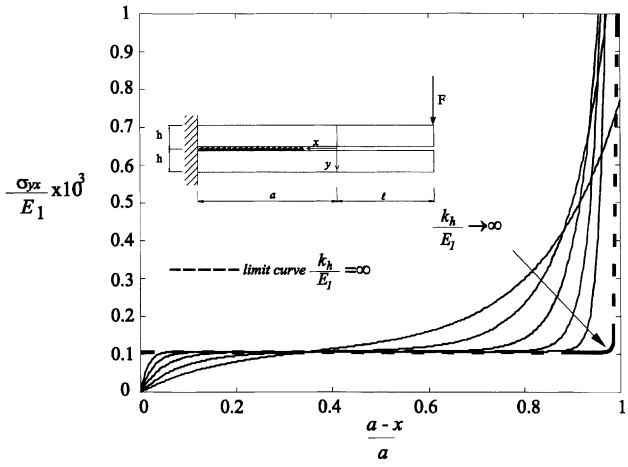

Fig. 16. Interlaminar shear stresses behaviour for k_h approaching infinity.

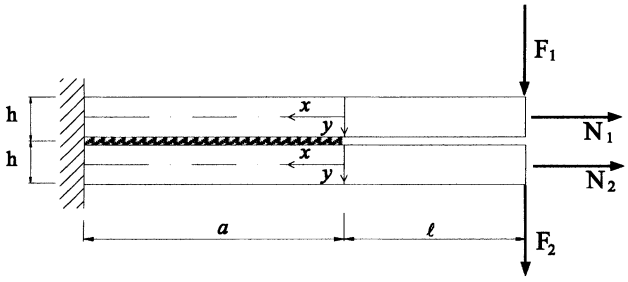

Fig. 17. Mixed mode loading system for the symmetrical two-layer scheme.

$$\begin{aligned}
&D\Delta\psi'' - A^*\Delta\psi - A^*\Delta w' = 0,\\
&A^*\Delta\psi' + A^*\Delta w'' - 2k_v\Delta w = 0,\\
&\Delta\psi(a) = 0, \Delta\psi'(0) = \frac{M_2 - M_1}{D},\\
&\Delta w(a) = 0, \Delta w'(0) + \Delta\psi(0) = \frac{T_2 - T_1}{A^*},
\end{aligned} \tag{29}$$

where $\Delta\psi = \psi_2 - \psi_1$ and $M_1 = -F_1 l, M_2 = -F_2 l, T_1 = -F_1, T_2 = -F_2$. The above posed problem is of the same nature as the problem formulated by Eqs. (13) and (14). The mode I component of energy release rate, for the particular geometrical scheme at hand, is thus governed by the normal interface stiffness and by the difference in bending moments and shear forces acting at the crack tip. Axial forces do not affect mode I fracture energy. For general geometrical configurations this is not true.

In general the problem must be faced by a numerical approach similar to that in mode I test example, but for a/h approaching infinity it is possible to get an analytical solution. This limit behaviour of the system is useful to understand well the general solution. By the same consideration made for mode I test we found that

$$\lim_{k_v\to\infty}\Delta w'(0)=\frac{M_2-M_1}{\sqrt{A^*D}}+\frac{T_2-T_1}{A^*},$$
$$\lim_{k_v\to\infty}\Delta\psi(0)=-\frac{M_2-M_1}{\sqrt{A^*D}}. \tag{30}$$

Thus the function $\Delta w'$ goes to zero for $0<x\leqslant a$, with a discontinuity at $x=0$, while $\Delta\psi_1$ tends toward the function $\Delta\psi(0)e^{-\sqrt{\frac{A^*}{D}}x}$. The non-zero relative rotation between the layers is responsible for bending/shear interaction arising from the work of shear stresses on section rotation along a closed path enclosing the crack tip. The energy release rate mode I component can be thus calculated

$$G_{\mathrm{I}}=\lim_{k_v\to\infty}\frac{1}{2B}k_v\Delta w(0)^2=\frac{1}{4B}\left(\frac{M_2-M_1}{\sqrt{D}}+\frac{T_2-T_1}{\sqrt{A^*}}\right)^2$$
$$=\frac{(M_2-M_1)^2}{4DB}+\frac{(T_2-T_1)^2}{4A^*B}+\frac{(M_2-M_1)(T_2-T_1)}{2B\sqrt{A^*D}}. \tag{31}$$

Energy release rate mode I component depends only on the difference in bending moments and shear forces.

The mode II component of fracture energy can be evaluated once the following problem is solved:

$$\Delta u''-(\frac{h^2}{2D}+\frac{2}{A})k_h\Delta u-\frac{h(T_1+T_2)}{2D}=0,$$
$$\Delta u(a)=0, \tag{32}$$
$$\Delta u'(0)=\frac{h(M_1+M_2)}{2D_1}+\frac{N_1-N_2}{A},$$

which gives the following solution:

$$\Delta u=\frac{\sqrt{A}he^{-\alpha\sqrt{k_h}x}}{2k_h(4D+Ah^2)(1+e^{2\alpha a\sqrt{k_h}})}\Bigg[(e^{2\alpha a\sqrt{k_h}}-e^{2\alpha\sqrt{k_h}x})$$
$$\times 2\alpha\sqrt{k_h}\left(M_1+M_2+2D\frac{N_1-N_2}{Ah}\right)$$
$$-2\sqrt{A}(e^{\alpha a\sqrt{k_h}}-e^{\alpha x\sqrt{k_h}})(e^{\alpha\sqrt{k_h}(a+x)}-1)(T_1+T_2)\Bigg], \tag{33}$$

where $\alpha^2=h^2/2D+2/A$. The energy release rate mode II component can be thus calculated

$$G_{\mathrm{II}}=\lim_{k_h\to\infty}\frac{1}{2B}k_h\Delta u(0)^2$$
$$=\frac{3}{16BD}\left[(M_1+M_2)+2D\frac{(N_1-N_2)}{Ah}\right]^2. \tag{34}$$

As we can observe, bending/shear interaction phenomenon affects only mode I component of energy release rate for this simplified scheme and the energy release rate mode II component is independent of the a/h ratio. Moreover, the mismatch in axial forces leads only to activate mode II component.

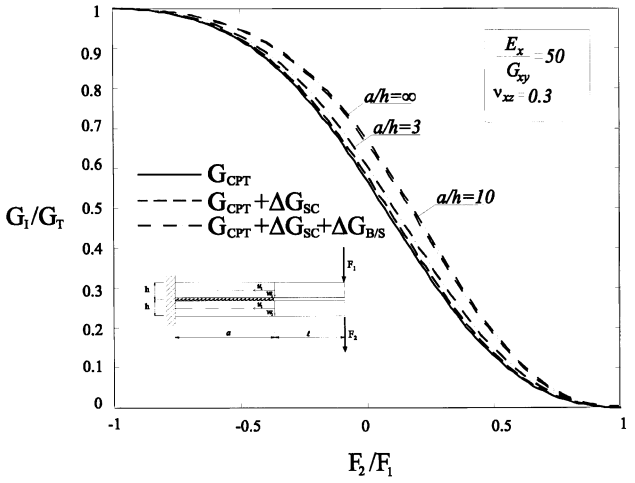

Fig. 18. Coupling ratio $G_{\mathrm{I}}/G_{\mathrm{T}}$ for different kinds of energy release rate approximation.

The coupling ratio $G_{\mathrm{I}}/G_{\mathrm{T}}$ plotted versus the F_2/F_1 ratio is shown in Fig. 18 for an ALDCB scheme with the same geometrical and mechanical parameters as mode I example: various kinds of approximation are taken into consideration. In this figure the following meaning for the different energy release rate terms are adopted on the hypothesis of a/h approaching infinity

$$G_{\mathrm{CPT}}=\frac{(M_2-M_1)^2}{4DB}+\frac{3}{16BD}\Bigg[(M_1+M_2)$$
$$+2D\frac{(N_1-N_2)}{Ah}\Bigg]^2,$$

$$\Delta G_{\mathrm{SC}}=\frac{(T_2-T_1)^2}{4A^*B},$$

$$\Delta G_{\mathrm{B/S}}=\frac{(M_2-M_1)(T_2-T_1)}{2B\sqrt{A^*D}}.$$

6. Conclusions

In this paper an analysis of delamination in plates is developed to perform the mode partition of the energy release rate.

The mechanical model here used is based on an interface model in which the adhesion between layers is modelled by means of linear elastic interface acting in the opening and sliding directions.

This model is useful to capture the essential features of the phenomenon and in the understanding of the complex behaviour of delamination failure. Moreover, it should be useful in view of further developments concerning FEM analysis of two-dimensional delamination problems. In this case, the adhesion between layers

could be modelled by means of a linear interface model able to transfer opening, sliding and tearing interlaminar stresses, thus defining local mode components of the energy release rate in a similar manner to that proposed in the present work.

The analysis has been developed by using Mindlin plate kinematics to model each layer. The solution given for the energy release rate shows the significant influence of shear deformation that, if neglected, can produce a notable overestimation of the actual strength of a delaminated plate.

Utilising a shear deformable layer-wise plate theory coupled with a linear interface model leads to evidencing the so-called stress interaction in energy release rate determination. To the authors' knowledge there are no works which point out this interesting behaviour, useful in understanding well the actual effect of shear deformation on the mechanism of plate delamination.

Among the important new features found in the previous analysis, the following should be underlined:

- The influence of shear cannot be circumscribed only to the standard terms T^2/BA^* but additional terms must also be accounted for arising from the so-called normal/shear stress interaction; this behaviour can have an important effect on the energy release rate evaluation, especially for laminates with low shear to bending stiffness ratio.
- Normal/shear interaction contributions to the energy release rate arise from asymptotic terms in the expansion of interlaminar stresses at the crack tip for the shear loading condition. From a mechanical point of view the above contribution arises because of the discontinuity of the derivative of axial displacements in the thickness direction at the interface between layers at the crack tip. This is evidenced by means of a modified application of the J-integral technique.
- In the case of a two-layer symmetrical scheme subjected to a general loading system it is possible to say that: differences in axial forces give rise to only mode II fracture energy; differences in bending moments activate only the mode I component while the mode II component is linked to the algebraic sum of moments; shear forces activate only the mode I component and bending/shear interaction affects only the mode I component.

References

[1] Bruno D. Delamination buckling in composite laminates with interlaminar defects. Theor Appl Fract Mech 1988;9:145–59.
[2] Bruno D, Greco F. An asymptotic analysis of delamination buckling and growth of layered plates. Int J Solids Struct 2000;37:6239–76.
[3] Houssan AT, William G. Durability characteristics of concrete beams externally bonded with FRP composite sheets. Cem Concr Compos 1997;9:351–8.
[4] Hutchinson JW, Suo Z. Mixed mode cracking in layered materials. In: Advances in Applied Mechanics, vol. 28. New York: Academic Press; 1992.
[5] Jones R, Paul J, Tay TE, Williams JF. Assessment of the effect of impact damage im composites: some problems and answers. Theor Appl Fract Mech 1988;9:83–95.
[6] Shapery RA, Davidson BD. Prediction of energy release rate for mixed-mode delamination using classical plate theory. Appl Mech Rev 1990;43:S281–7.
[7] Suo Z, Hutchinson JW. Interface crack between two elastic layers. Int J Fract 1990;43:1–18.
[8] Allix O, Ladevèze P, Corigliano A. Damage analysis of interlaminar fracture specimens. Compos Struct 1995;31:61–74.
[9] Williams JG. On the calculation of energy release rates for cracked laminates. Int J Fract 1988;36:101–19.
[10] Kanninen MF. An augmented double cantilever beam model for studying crack propagation and arrest. Int J Fract 1973;9:83–91.
[11] Chang DJ, Muki R, Westmann RA. Double cantileverb beam models in adhesive mechanics. Int J Solids Struct 1976;12:13–26.
[12] Ascione L, Bruno D. On the delamination problem of two-layer plates. In: Proceedings of the Second Meeting on Unilateral Problems in Structural Analysis, Ravello, 22–24 September 1983, CISM Courses and Lectures No. 288. Berlin: Springer.
[13] Bruno D, Greco F. An analysis of mixed mode delamination in plates. Int J Solids Struct, submitted.
[14] Chatterjee SN, Kulkarni SV. Shear correction factors for laminated plates. AIAA J 1979;17(5):498–9.